J. Fluid Mech. (1970), *vol.* 42, *part* 4, *pp.* 823–844
Printed in Great Britain

Measurements in a three-dimensional turbulent boundary layer induced by a swept, forward-facing step

By JAMES P. JOHNSTON
Mechanical Engineering Department, Stanford University

(Received 6 October 1969)

An experiment is reported, in which turbulent shear-stresses as well as mean velocities have been measured in a three-dimensional turbulent boundary layer approaching separation. It is shown that even very close to the wall the stress vector does not align itself with the mean velocity gradient vector, as would be required by a scalar 'eddy viscosity' or 'mixing length' type assumption. The calculation method of Bradshaw (1969) is tested against the data, and found to give good results, except for the prediction of shear-stress vector direction.

1. Introduction

The primary purpose of this paper is to report the results of a three-dimensional turbulent boundary-layer experiment, in which vector profiles of the turbulent shear-stress were obtained in addition to those of mean velocity. The need for measurements of this type has been expressed by Bradshaw (1969) and Nash (1969), both of whom have recently developed methods for solution of the incompressible turbulent boundary-layer equations on flat or slightly curved surfaces in regions far from edge or corner effects.

These methods are very different from earlier methods (e.g. Cumpty & Head 1967), which use boundary-layer integral equations and require empirical input on mean velocity profile shapes. It has become increasingly evident, as shown by Klinksiek & Pierce (1969), that current proposals for representing cross-flow velocity profiles in terms of a small number of parameters are not satisfactory. Hence, the hope for construction of a general, integral equation method appears dim at present.

The methods of Bradshaw (1969) and Nash (1969) are basically similar in that both involve numerical integration of boundary-layer differential equations which contain as unknowns the components τ_x and τ_y of the turbulent shear-stress vector. In both methods an equation based on the turbulent energy equation is used to describe the evolution of the magnitude of the shear-stress along a mean flow streamline. The empirical functions of Bradshaw, Ferriss & Atwell (1967) are carried over directly in their two-dimensional form. The basic difference in the methods lies in the assumptions regarding the *direction* of the shear-stress vector.

If rectangular Cartesian co-ordinates (x, y, z), where y is normal to the wall, are used to define the mean (U, V, W) and fluctuating (u, v, w) components of velocity, then $\tau_x = (-\rho\overline{uv})$ and $\tau_z = (-\rho\overline{wv})$ are the components of turbulent shear-stress in the x and z directions. The two major gradients of mean velocity $\partial U/\partial y$ and $\partial W/\partial y$, the components of the mean velocity gradient vector, define the direction of mean rate of strain in a boundary layer. Nash argues that the shear-stress is likely to act in the mean rate of strain direction, so his closure equation is simply

$$\tau_x/(\partial U/\partial y) = \tau_z/(\partial W/\partial y). \tag{1}$$

The same equation results from a scalar 'eddy viscosity' or 'mixing length' model. On the other hand, Bradshaw's equations for the shear-stress components permit the shear-stress vector to deviate from the strain rate direction. His form results from arguments concerning the relative effects of the 'pressure-strain', 'dissipation' and 'diffusion' terms in the equations for the rates of change of the turbulence stresses $(-\rho\overline{uv})$ and $(-\rho\overline{wv})$ which are derivable from the Navier–Stokes equations (see Townsend 1956, ch. 2). Arguments for either method are based on slender evidence. The research, upon which this paper is based, was intended to provide some direct shear-stress vector measurements throughout the depth of a three-dimensional turbulent boundary layer, so that some understanding of the facts of the situation might be obtained.

The only other measurements of this sort (known to the author) are those of Bradshaw & Terrell (1969), also partially reported by Bradshaw (1969). In their experiment, measurements were made of velocity and shear-stress vectors on a flat plate attached to the trailing edge of a 45° 'infinite' swept wing. Small cross-flow was produced in the layer by the pressure field of the wing. The region of measurement extended downstream of the airfoil where, by the action of shear-stress alone, the cross-flow decays and the streamwise flow returns to constant-pressure equilibrium conditions. The results of these measurements tend to confirm Bradshaw's (1969) method. However, in the inner third of the layer, the hypothesis represented by (1) appears to be confirmed by both experiment and theory.

The experiment conducted for this report produced conditions that severely tested this hypothesis in the region close to the wall above the laminar sublayer. In essence, a thick, two-dimensional turbulent boundary layer was forced to flow towards an 'infinite' 45° swept step. The adverse pressure gradients imposed on the layer as it approached the step caused cross-flow to develop. The cross-flow became large close to the wall and near the separation line which occurred ahead of the step. Although not a particularly good test case for the theories, since the mean flow development depends far more on the pressure gradients than on shear-stress gradients, the experiments revealed that a substantial deviation existed between the shear-stress and mean velocity gradient directions throughout the inner as well as the outer parts of the outer flow.

The experimental programme and methods are discussed in §§2–4. The final results are discussed and compared to calculations made with Bradshaw's method in §§5 and 6.

2. Apparatus and general procedure

The experimental programme was accomplished in two phases. The first phase, described in § 3, defined the mean flow field. The principal results of these measurements were profiles of total mean velocity Q, yaw angle θ, and pitch angle β (see figure 3). The second phase, to measure turbulence intensity and shear-stress components, is described in § 4. This article provides a brief review of the main features of the apparatus and the general experimental procedure.

The low turbulence wind tunnel described by Bradshaw (1965) was used with a modified 10 in. by 15 in. test section (figure 1). A 2 in. high rectangular step, swept at 45°, was installed on the test section floor.

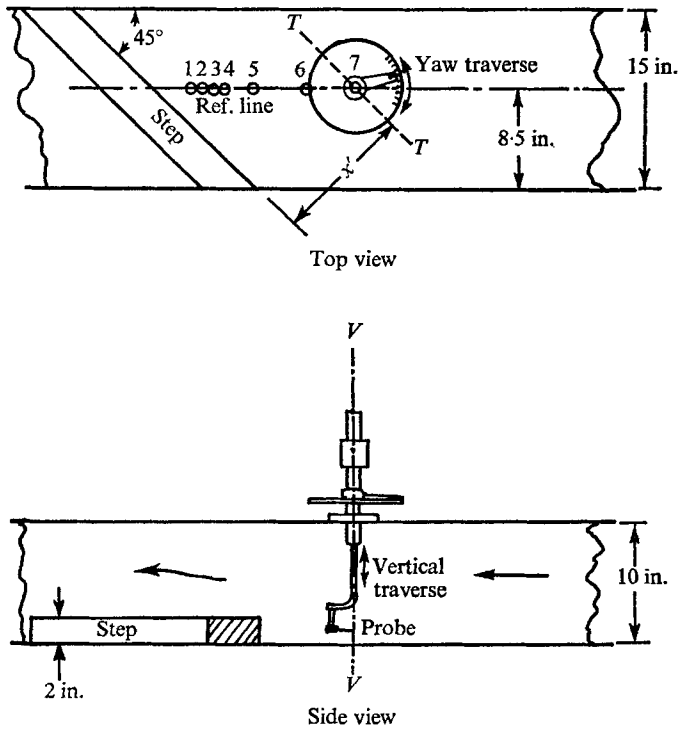

FIGURE 1. Test section and step. Traverse location at station 1 ($x' = 2{\cdot}25$ in.), 2 ($x' = 3{\cdot}00$ in.), 3 ($x' = 3{\cdot}75$ in.), 4 ($x' = 4{\cdot}50$ in.), 5 ($x' = 6{\cdot}00$ in.), 6 ($x' = 9{\cdot}00$ in.) and 7 ($x' = 12{\cdot}00$ in.).

The air in the test section was nominally at room temperature and atmospheric pressure. The reference speed of $U_{\text{ref}} = 104$ ft./sec was based on the reference dynamic pressure, $\frac{1}{2}\rho U_{\text{ref}}^2 = (P_\infty - p_{\text{ref}})$, held constant for all tests. P_∞ is the free-stream total pressure and p_{ref} the wall static pressure measured in the 10 in. by 15 in. inlet duct at a reference point 20 in. upstream of the first profile measurement station, no. 7. The nominal unit Reynolds number for the tests was $6{\cdot}1 \times 10^5$ (1/ft.).

The boundary layer was measured upstream of the step and over the floor

of the test section. The floor was instrumented with wall static pressure taps located along, and to either side of, the reference line. The top wall was made of a number of plates cut at the same angle as the step, 45°. The probe traversing gear, mounted on one of the top plates, could be located at seven different distances x' relative to the step. The whole traversing gear could be moved parallel to the step, e.g. along line TT in figure 1.

The positions x' of the seven traversing locations were selected after some preliminary measurements of wall-trace streaks left on an oil and titanium dioxide film applied to the tunnel floor. Station 1, at $x' = 2{\cdot}25$ in., was located just ahead of the flow separation zone, forward of the step. Station 7, at $x' = 12{\cdot}00$ in., was located where the flow was essentially two-dimensional and parallel to the reference line. At station 7, the boundary layer was 2·3 in. thick. The wall-trace streaks indicated that the flow close to the wall was independent of position parallel to the step over a region of at least ± 3 in. to either side of the reference line. The wall flow thus approximated conditions of flow over an 'infinite' swept body. In order to be in the region of 'infinite' swept flow, all reported profile measurements were obtained with the measurement stations located on the reference line.

The probe traversing gear could move vertically and in yaw. Two different probe holding stems were used, one (figure 2(*a*)) for pressure probes and the other (figure 2(*b*)) for hot wire probes. The latter held the probe axis at a 6° pitch angle to permit the probe tip to approach the wall closely. The yaw angle could be measured to $\pm 0{\cdot}3°$ relative to the reference line, the vertical position of pressure probes was measured to $\pm 0{\cdot}001$ in. and hot wire probes to $\pm 0{\cdot}01$ in.†

For the purpose of determining the effects of pitch on the probes, the traversing gear could be mounted on a device that allowed variation and measurement of the pitch angle of a probe over a range of $\pm 15°$ relative to the tunnel floor. The device was used with the swept step removed from the tunnel when the probe under calibration was located in the central, uniform core of the flow.

Pressures were read on a precision, multitube, alcohol filled manometer inclined at 20° to the horizontal and a type P-5D Statham pressure transducer. The basic uncertainty in pressure readings was estimated to be $\pm 0{\cdot}003$ vertical inches of water. Pressures were read relative to the reference static pressure p_{ref} or free stream total pressure P_∞ and normalized on the constant dynamic pressure, $\frac{1}{2}\rho U_{\mathrm{ref}}^2 = (P_\infty - p_{\mathrm{ref}})$, to form pressure coefficients that had minimum uncertainties of $\pm 0{\cdot}002$.

Two types of hot wire probes were used: a normal, single-wire probe and a Disa miniature X-wire probe, type 55A38 whose manufactured dimensions were: wire length 1·2 mm, wire separation 0·2 mm and angle between wires $90 \pm 3°$. Two Disa 55A01 constant temperature hot wire anemometers and the signal processing equipment (multiplier, differential amplifier, integrator, etc.) of the NPL Aerodynamics Division (see Bradshaw & Johnson 1963) were used to control, process and read out the hot wire signals. Calibration of the wires and

† The pressure probes were located by electric contact with the wall, whereas the hot wires were located by visual observation relative to a machinist's scale held against the wall.

signal processing equipment was conducted each time a traverse of the boundary layer was conducted.

Probably the most serious source of error in the hot wire measurements was the uncertainty in the effective cosine cooling law angles of the wires in the X-wire probe. Calibrations to determine these angles were conducted by pitching the probe in the tunnel free-stream and noting output voltage as a function of angle for all expected pitch angles $\pm 6°$ relative to the probe axis. The accuracy of the measurements, which were accomplished by differentiation of the voltage-angle curves, was not sufficient to detect deviations from the cosine cooling law. The range of possible error in effective, calibrated wire angles was estimated to be $\pm 2°$.

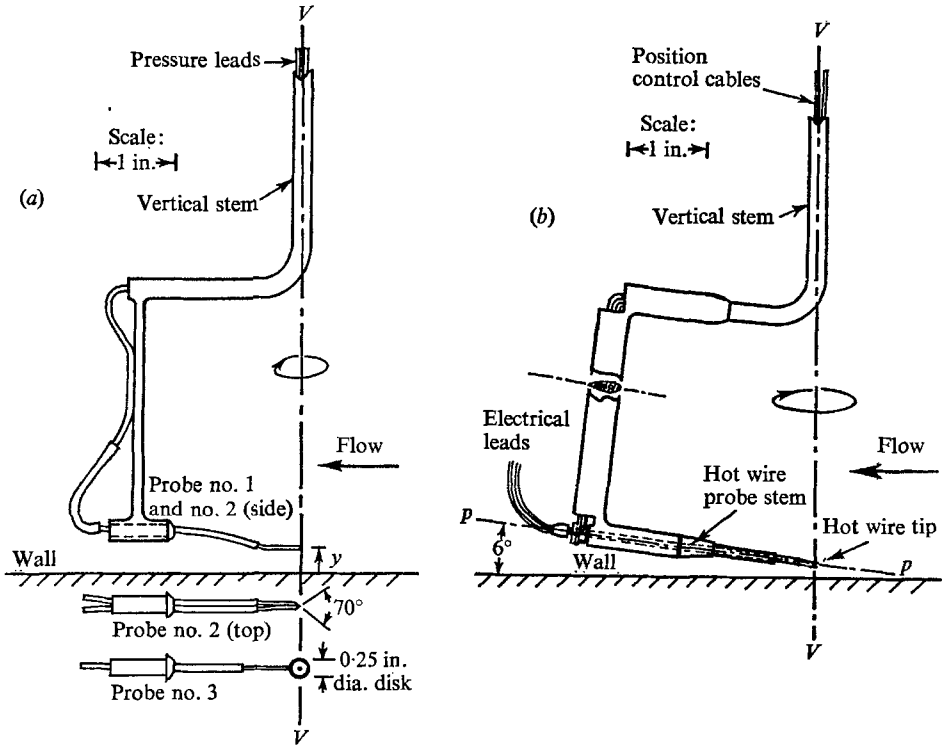

FIGURE 2. Traversing, probe holding stems and probes. y and θ motion along and around axis V–V. (*a*) Pressure probes and stem. (*b*) Hot wire stem; line p–p is probe axis.

3. Mean flow measurements

The first mean flow measurements established the wall static pressure distribution ahead of the step (figure 4). Measurements of wall static pressure out to ± 3 in. on either side of the reference line showed that spanwise (along the step) variation of pressure was less than $0{\cdot}01(\frac{1}{2}\rho U_{\text{ref}}^2)$. C_p attained a nearly constant, maximum value of 0·14 at $x' = 1{\cdot}5$ in. out from the step. The forward flow separation line was located using a fine wool tuft on a thin rod. It lay roughly at $x' = 1{\cdot}5$ in. which is consistent with the location of maximum pressure recovery.

Because the air had to sweep up over the step, there was substantially greater mean streamline curvature than normal in the outer $\frac{3}{4}$ of a boundary layer. As a result, strong gradients of static pressure normal to the wall occurred in the layer; especially in the regions close to the separation line where the interesting three-dimensional aspects of the flow were the largest. It was thus necessary to measure profiles of static pressure, as well as total pressure, to allow deduction of mean velocity magnitude profiles.

The traversing stem shown in figure 2(*a*) was designed to hold various pressure probes. Among those used were the three illustrated: no. 1 (a round impact

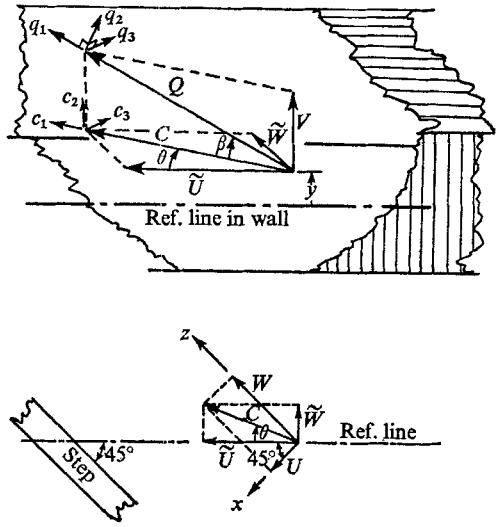

FIGURE 3. Velocity components and angles.

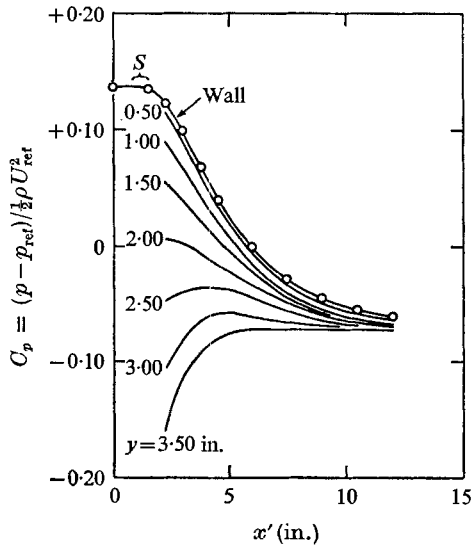

FIGURE 4. Static pressure coefficient. *S* marks separation point location.

pressure tube of 0·025 in. O.D.), no. 2 (a Conrad tube made from two, 0·025 in. O.D. tubes soldered side by side and cut off at the tip with a 70° apex angle), no. 3 (a thin, flat, disk-static probe made as close as possible in geometry to that illustrated in figure 1(*h*) of Bryer, Walshe & Garner 1955). A fourth probe, an impact tube pitched at 10° to the wall, was used to demonstrate that errors due to pitch angle on no. 1 probe were negligible.

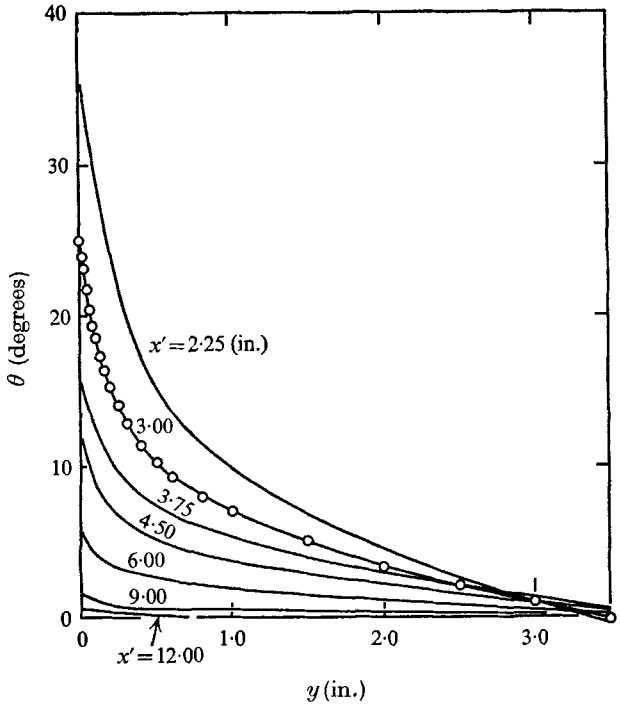

FIGURE 5. Yaw angle θ. Typical data points shown on $x' = 3{\cdot}00$ in. curve.

No. 2 probe, with the two tubes set parallel to the wall, was used to obtain yaw angle θ. The stem was rotated, at each profile point, until zero pressure differential was obtained across the two tubes. Small calibrated corrections for angular runout† of the traversing gear ($< 1{\cdot}5°$) and local pitch effects ($< 1{\cdot}0°$) were applied to obtain the final yaw results shown in figure 5. For $y > 0{\cdot}5$ in., the uncertainty of these results is less than $\pm 0{\cdot}5°$, but very near the wall, the uncertainty may be as high as $\pm 1{\cdot}0°$.

The limiting wall streamline angles (figure 6) were obtained by extrapolations of the results in figure 5 to $y = 0$. Continuation of the angles θ_w, to 45° tends to indicate that limiting wall streamlines become parallel to the separation line in the manner described as 'ordinary separation' by Maskell (1955). This observation is consistent with observations made of the streaks in the preliminary oil-film studies. The oil flow streaks appeared to approach the separation line from both sides in a tangential manner.

† The built-in reference angle error which varies with position y. It is caused by manufacturing tolerances and wear in the traversing gear.

Profiles of total pressure were measured with probe no. 1. At each profile point, the probe was aligned in the local yaw direction. Selected results from the total pressure profiles are shown in figure 7 (*a*).

As the yaw angle had already been measured, it was possible to align the disk-static probe in the local yaw direction. The probe had the characteristic that its calibration factor $k = 0{\cdot}08$, where $k = (p - p_{\text{ref}})/\frac{1}{2}\rho Q^2$, was insensitive to pitch angle over the whole range of calibration ($-10°$ to $+15°$) and yaw angle to $\pm 2°$. The yaw insensitive range was large enough to assure proper operation for all probe displacements of $y > 0{\cdot}25$ in. In addition, k was shown to be insensitive to Reynolds number effects in the range of test conditions and final check runs showed that $k = 0{\cdot}08 \pm 0{\cdot}01$ through the whole depth of the 2·5 in. thick turbulent layer obtained on the tunnel floor with the step removed.

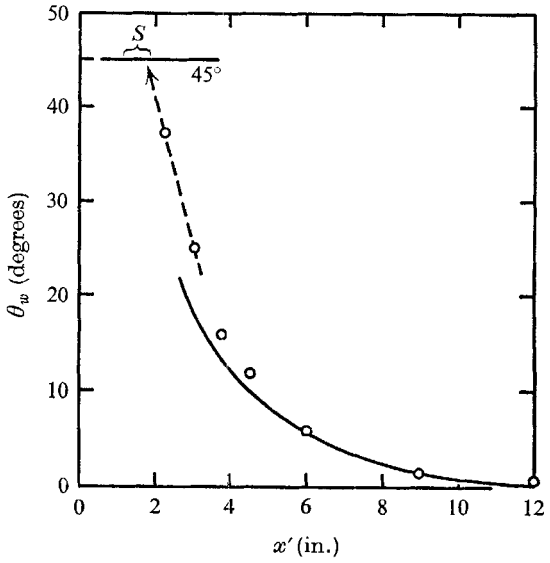

FIGURE 6. Limiting wall streamline angle θ_w. Solid curve calculated by method of §5. S marks separation point location.

The final static pressure results are shown in figure 4, where C_p is plotted as a function of y and x'. In the inner layers, $y < 1{\cdot}0$ in., the streamwise positive pressure gradients are nearly independent of y. However, the pressure gradients become negative far from the wall. As a consequence of the nearly inviscid behaviour of the outer flow, the negative streamwise pressure gradient implies some acceleration of the free-stream velocity (see values for Q for $y \geqslant 3{\cdot}0$ in. in figure 8) and, for flow over the forward part of an 'infinite' swept body, some negative yaw is also expected and observed (see θ at $y = 3{\cdot}5$ in. in figure 5).

The mean velocity magnitude Q profiles deduced from the measured total and static pressure profiles are shown in figure 8. The free-stream velocity at all seven traversing stations is slightly greater than the upstream reference velocity due to the 'effective' slow convergence of the test section area caused by floor, roof and side wall boundary-layer growth.

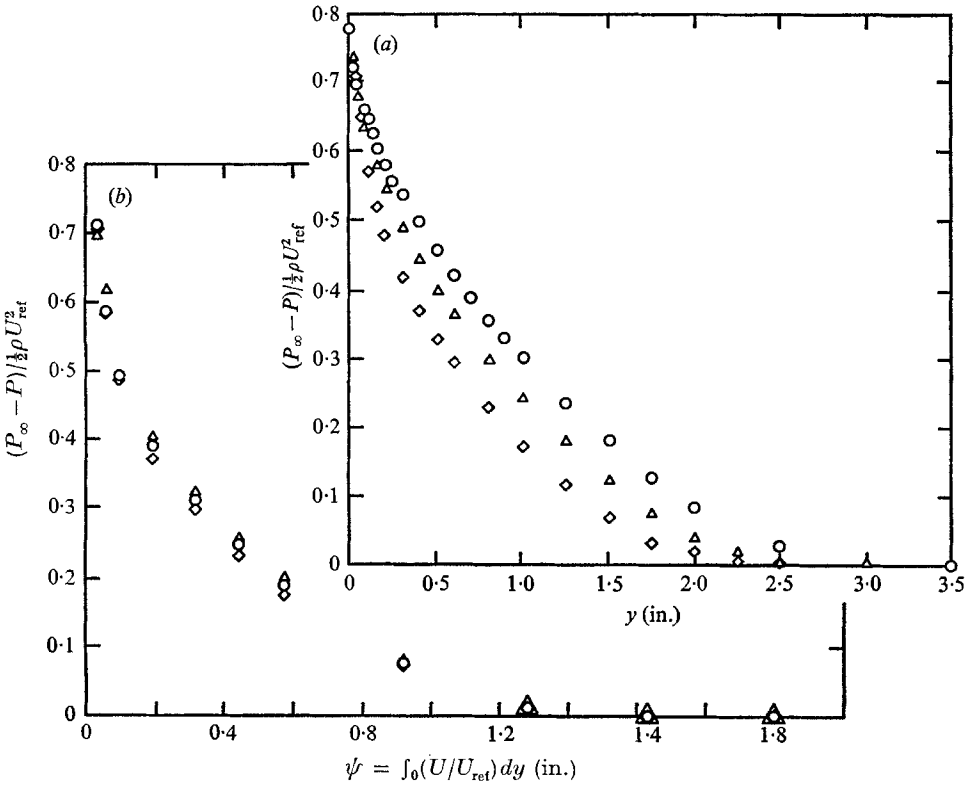

FIGURE 7 (*a*), (*b*). Typical total pressure loss coefficient data: ◇, $x' = 12{\cdot}00$ in.; △, 4·50 in.; ○, 3·00 in.

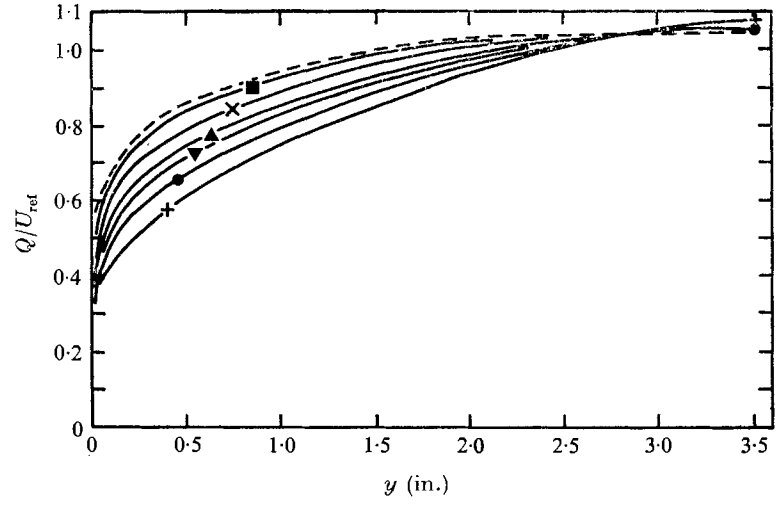

FIGURE 8. Velocity magnitude, Q. No data points shown. +, $x' = 2{\cdot}25$ in.; ●, 3·00 in.; ▼, 3·75 in.; ▲, 4·50 in.; ×, 6·00 in.; ■, 9·00 in.; ----, 12·00 in.

Measurement of pitch angle β was accomplished using the Conrad probe, no. 2, set on edge in the traversing stem so the two tubes lay in a plane perpendicular to the wall. When the probe tip was set at the local yaw angle, the pitch angle was determined by measurement of the differential pressure Δp between the two tubes. The probe pressure coefficient $\Delta p/\frac{1}{2}\rho Q^2$ varied linearly with pitch angle according to initial calibration in the free-stream. Small corrections ($< 1°$) had to be applied to obtain the final results shown in figure 9 in order to account for the effects of vertical gradients of dynamic pressure in the boundary layer. The estimated uncertainty in β is $\pm 0{\cdot}5°$.

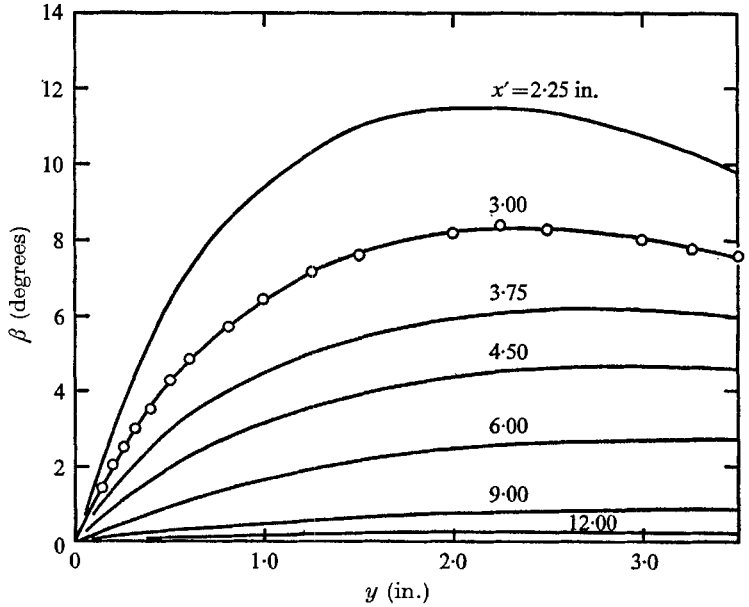

FIGURE 9. Pitch angle β. Typical data points shown on $x' = 3{\cdot}00$ in. curve.

Values of the wall shear-stress τ_w were estimated from the mean velocity profile measurements using the law of the wall in the form

$$\frac{Q}{(\tau_w/\rho)^{\frac{1}{2}}} = 5{\cdot}6 \log_{10}\left(\frac{y(\tau_w/\rho)^{\frac{1}{2}}}{\nu}\right) + 4{\cdot}9.$$

Use of the developed mean velocity rather that Q in the formula as suggested by Perry & Joubert (1965) gave nearly identical results. A recent note by Pierce & Krommenhoek (1968) suggests, on the basis of some direct wall force measurements in a roughly similar type of three-dimensional turbulent boundary layer, that this method may give τ_w values that are $\sim 10\%$ too high. Subsequent measurements† using a Preston tube substantiated this conclusion. Figure 10 is shown to illustrate the degree of fit of the present data to the law of the wall formula. No corrections for effective displacement of the impact tube centre have been applied.

† By Bradshaw in 1968 on my original apparatus.

Figure 11 shows the wall shear-stress as a function of distance from the step. Even if the values of τ_w were reduced by 10%, it does not appear that the stress would extrapolate to zero at the separation line. This is further evidence of the 'ordinary' nature of the separation; under such conditions the wall stress is not required to be zero.

The hodograph plots of the mean velocity vector projection in the wall plane

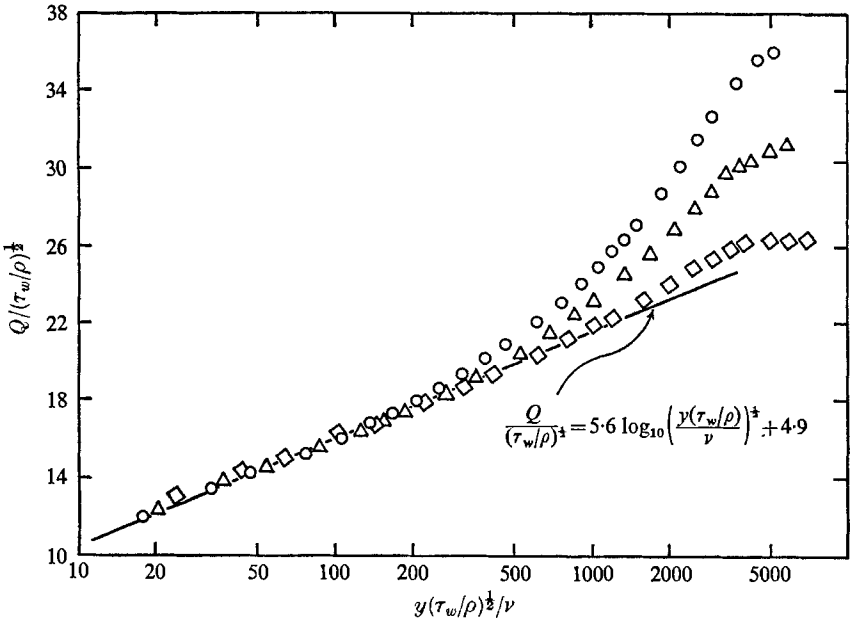

FIGURE 10. Law of the wall plot of velocity magnitude data: ○, $x' = 3{\cdot}00$ in.; △, 4·50 in.; ◇, 12·00 in.

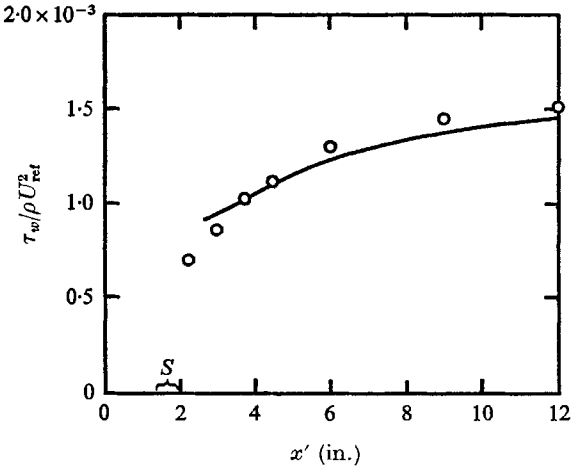

FIGURE 11. Wall shear stress. Solid curve calculated by method of §5. S marks separation point location.

are shown in figure 12. Peak values of $\tilde{W}$, the cross-flow velocity, occurred between $y = 0{\cdot}03$ and $0{\cdot}07$ in. from the wall at $y(\tau_w/\rho)^{\frac{1}{2}}/\nu$ values of 60–100. The angles of the mean velocity gradient vector (see figures 18(*a*), (*b*)) were obtained from the slopes of the curves in figure 12. In the outer flow, the rapid change of $\tilde{W}$ with respect to $\tilde{U}$ is thought to be associated with the nearly potential nature of the flow over the step. Similar effects can be seen in the hodograph plots of the data of Joubert, Perry & Brown (1967) (see their figure 8), for a three-dimensional turbulent layer generated by a hill on a flat plate.

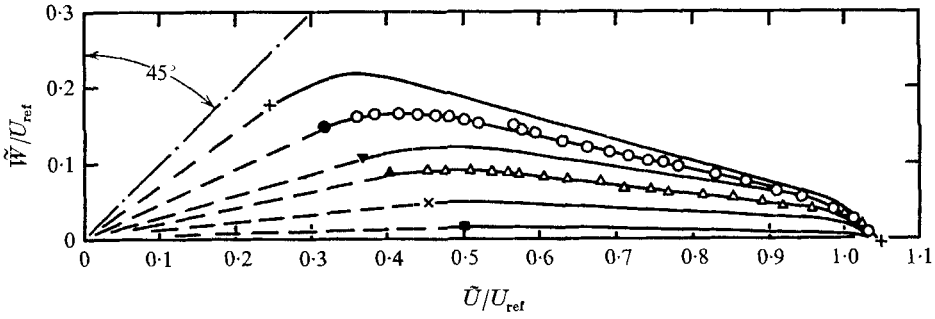

FIGURE 12. Hodograph plot of $\tilde{W}$ *vs.* $\tilde{U}$: +, $x' = 2{\cdot}25$ in.; ●, 3·00 in.; ▼, 3·75 in.; ▲, 4·500 in.; ×, 6·00 in.; □, 9·00 in. Typical data points shown on curves for $x' = 3{\cdot}00$ in. and 4·50 in.

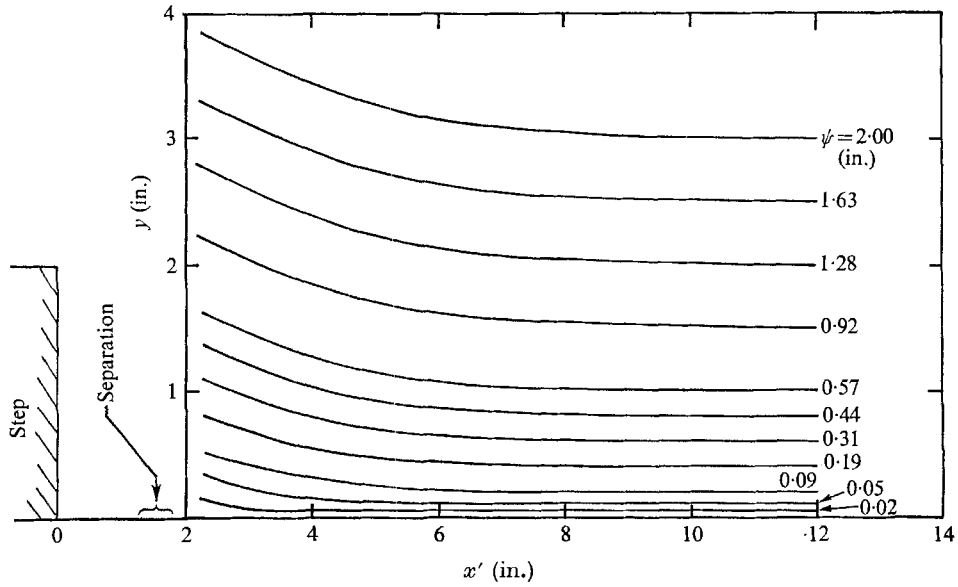

FIGURE 13. Stream function contours in the x'–y plane—normal to the step.

Because of the greater than normal pitch in the experimental boundary layer, mean streamlines were not lines of nearly constant y. Some of the results are more easily interpreted when their values are examined for changes along streamlines. Hence, it was desired to plot some of the results against the stream function

ψ rather than y. Assuming the flow in the region of measurement is equivalent to the flow over an 'infinite' swept body, ψ was determined from the mean velocity profiles, using

$$\psi = \int_{y=0} \left[\frac{U}{U_{\text{ref}}}\right] dy = \int_{y=0} \left[\frac{Q \cos\beta \cos(\theta + \frac{1}{4}\pi)}{U_{\text{ref}}}\right] dy.$$

Figure 13 shows contours of constant ψ in the y–x' plane.

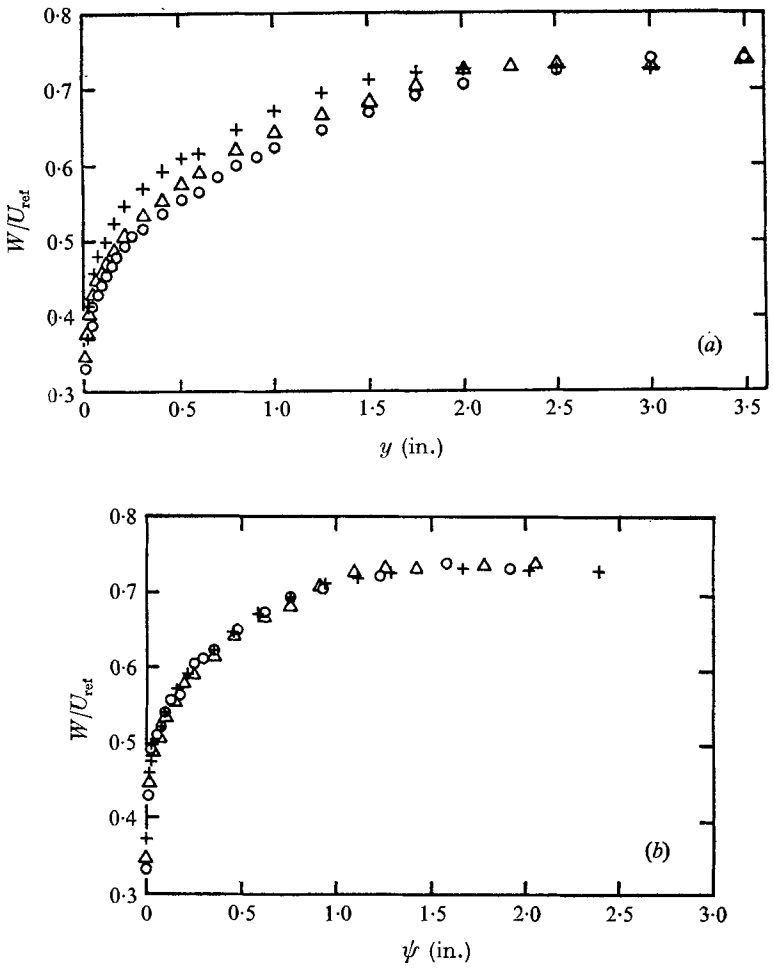

FIGURE 14(*a*), (*b*). Step-parallel velocity component profiles: +, $x' = 12{\cdot}00$ in.; △, 4·50 in.; ○, 3·00 in.

Figures 14(*a*) and (*b*) illustrate the value of ψ as an independent parameter for profile plots. The velocity component W parallel to the step is shown *vs.* y in figure 14(*a*), and ψ in 14(*b*). In 14(*b*) all profiles collapse to a common curve, as expected for flow over an 'infinite' swept body where there are no net forces in the step-parallel direction to cause change of the W directed fluid particle momentum.

For flow of a thick turbulent boundary layer over a step set normal to the flow, there is, due to the rapid streamwise deceleration of the flow, very little change in total pressure P along mean streamlines, except very near the wall (Bradshaw & Galea 1967). A similar conclusion can be drawn from the data of this experiment as shown in figure 7 (b), where P is plotted against ψ rather than y as in figure 7 (a).

4. Turbulence measurements

For convenience, the three mutually perpendicular velocity fluctuation components q_1, q_2 and q_3 (see figure 3) were measured. The longitudinal component q_1 parallels the direction of the mean velocity vector **Q**, and q_3 is defined to be parallel to the wall. The results are presented in terms of the components c_1, c_2 and c_3, along and perpendicular to **C**, the wall projection of the mean velocity vector **Q**. The equations relating these components are:

$$c_1 = q_1 \cos\beta - q_2 \sin\beta, \tag{2a}$$

$$c_2 = q_1 \sin\beta + q_2 \cos\beta, \tag{2b}$$

$$c_3 = q_3. \tag{2c}$$

The relationships between the components of the Reynolds stress for these two sets of components are:

$$\overline{c_1^2} = \overline{q_1^2}\cos^2\beta - 2\overline{q_1 q_2}\cos\beta\sin\beta + \overline{q_2^2}\sin^2\beta, \tag{3a}$$

$$\overline{c_2^2} = \overline{q_1^2}\sin^2\beta + 2\overline{q_1 q_2}\cos\beta\sin\beta + \overline{q_2^2}\cos^2\beta, \tag{3b}$$

$$\overline{c_3^2} = \overline{q_3^2}, \tag{3c}$$

$$\overline{c_1 c_2} = \overline{q_1 q_2}(\cos^2\beta - \sin^2\beta) + (\overline{q_1^2} - \overline{q_2^2})\cos\beta\sin\beta, \tag{3d}$$

$$\overline{c_3 c_2} = \overline{q_3 q_2}\cos\beta + \overline{q_3 q_1}\sin\beta, \tag{3e}$$

$$\overline{c_3 c_1} = \overline{q_3 q_1}\cos\beta - \overline{q_3 q_2}\sin\beta. \tag{3f}$$

The magnitude of the turbulent shear-stress is:

$$\tau = \rho[(-\overline{c_1 c_2})^2 + (-\overline{c_3 c_2})^2]^{\frac{1}{2}}, \tag{4}$$

and its direction relative to the reference line is

$$\theta_\tau = \theta + \arctan[(-\overline{c_3 c_2})/(-\overline{c_1 c_2})]. \tag{5}$$

The turbulence energy $\overline{q^2}/2$ is obtained from

$$\overline{q^2} = \overline{q_1^2} + \overline{q_2^2} + \overline{q_3^2} = \overline{c^2} = \overline{c_1^2} + \overline{c_2^2} + \overline{c_3^2}. \tag{6}$$

Profiles of the longitudinal turbulence intensity $\overline{q_1^2}$ were obtained at each of the seven traversing stations with the single wire probe mounted in the traversing stem, so that the wire was parallel to the wall. At each station and y position, the probe was set at the previously measured yaw angle so that the wire would be perpendicular to the mean velocity vector **Q**.

All other measurements were accomplished with the X-wire probe. The traversing stem was designed to allow the measurement of $\overline{q_1 q_2}$ and $\overline{q_3 q_2}$, the two princi-

pal contributions to the shear-stress components $-\rho(\overline{c_1c_2})$ and $-\rho(\overline{c_3c_2})$, by the quarter-squares method (Bradshaw & Johnson 1963). The quantities $\overline{q_2^2}$ and $\overline{q_3^2}$ were obtained by the regular cross-wire method.

Angular position of plane of wires about probe axis, pp	Position number	Wire number	Equation: e_{ij}, volts output, a_{ij} and b_{ij}, response coeffs., subscript i, position number., subscript j, wire number	Equation number
Perpendicular to the wall	1	1	$e_{11} = a_{11}q_1 + b_{11}q_2$	(7*a*)
		2	$e_{12} = a_{12}q_1 - b_{11}q_2$	(7*b*)
Rotated 180° relative to position number 1	2	1	$e_{21} = a_{21}q_1 - b_{21}q_2$	(7*c*)
		2	$e_{22} = a_{22}q_1 + b_{22}q_2$	(7*d*)
Rotated +45° relative to position number 1	3	1	$e_{31} = a_{31}q_1 + b_{31}(q_2 - q_3)/\sqrt{2}$	(7*e*)
		2	$e_{32} = a_{32}q_1 - b_{32}(q_2 - q_3)/\sqrt{2}$	(7*f*)
Rotated −45° relative to position number 1	4	1	$e_{41} = a_{41}q_1 + b_{41}(q_2 + q_3)/\sqrt{2}$	(7*g*)
		2	$e_{42} = a_{42}q_1 - b_{42}(q_2 + q_3)/\sqrt{2}$	(7*h*)
Rotated +90° relative to position number 1	5	1	$e_{51} = a_{51}q_1 - b_{51}q_3$	(7*i*)
		2	$e_{52} = a_{52}q_1 + b_{51}q_3$	(7*j*)

TABLE 1. Wire response equations for X-wire probe

To carry out the required operations, the crossed wire probe could be manipulated from outside the tunnel to rotate the probe stem about its axis (line pp in figure 2(*b*)) into any one of five different angular positions. The wire response equations (7*a*)–(7*j*) are shown in table 1, together with a description of the five positions. Ideally, the probe axis should always have been aligned with the mean velocity vector. Yaw alignment was achieved at every measuring point, but pitch variations had to be accounted for in the coefficients, a_{ij} and b_{ij}, of the response equations (table 1). The response equations were used to deduce the data reduction equations, which follow:

$\overline{q_2^2}$ was obtained by subtracting, squaring and averaging the output signals from wires 1 and 2 when the probe was in position 1. Equations (7*a*) and (7*b*) give the result,

$$\overline{q_2^2} = \frac{\overline{[(e_{11}-e_{12})^2]} - (a_{11}-a_{12})^2\overline{q_1^2} - 2(a_{11}-a_{12})(b_{11}+b_{12})\overline{q_1q_2}}{(b_{11}+b_{12})^2}. \tag{8}$$

$\overline{q_3^2}$ is similarly obtained with the probe in position 5, where the crossed wires are both nearly parallel to the wall. Equations (7*i*) and (7*j*) yield

$$\overline{q_3^2} = \frac{\overline{[(e_{51}-e_{52})^2]} - (a_{51}-a_{52})^2\overline{q_1^2} + 2(a_{51}-a_{52})(b_{51}+b_{52})\overline{q_3q_1}}{(b_{51}+b_{52})^2}. \tag{9}$$

$\overline{q_1q_2}$ was obtained by subtracting the mean square output of wire 1 while held in position 1 from its output in position 2. Equations (7*a*) and (7*c*), when they are squared, averaged and subtracted, give the equation,

$$\overline{q_1q_2} = \frac{\overline{[e_{11}^2 - e_{21}^2]} - (a_{11}^2 - a_{21}^2)\overline{q_1^2} - (b_{11}^2 - b_{21}^2)\overline{q_2^2}}{2(a_{11}b_{11} + a_{21}b_{21})}. \tag{10}$$

Finally, the quantity $\overline{q_3 q_2}$ was obtained by subtracting the mean squares of output differences $(e_{31}-e_{32})$ and $(e_{41}-e_{42})$ from the two wires when held successively in positions 3 and 4. Equations (7*e*)–(7*h*) give

$$\overline{q_3 q_2} = \frac{[\overline{(e_{31}-e_{32})^2}-\overline{(e_{41}-e_{42})^2}]}{-2(M_1+M_2)}+\frac{(L_1-L_2)\,\overline{q_1^2}}{2(M_1+M_2)}$$
$$+\frac{(M_1-M_2)(\overline{q_2^2}+\overline{q_3^2})}{2(M_1+M_2)}+\frac{(N_1-N_2)\,\overline{q_1 q_2}}{2(M_1+M_2)}+\frac{(N_1+N_2)\,\overline{q_3 q_1}}{-2(M_1+M_2)}, \tag{11}$$

where

$$L_1 = (a_{31}-a_{32})^2, \quad L_2 = (a_{41}-a_{42})^2,$$
$$M_1 = (b_{31}+b_{32})^2/2, \quad M_2 = (b_{41}+b_{42})^2/2,$$
$$N_1 = (a_{31}-a_{32})(b_{31}+b_{32})\sqrt{2}, \quad N_2 = (a_{41}-a_{42})(b_{41}+b_{42})\sqrt{2}.$$

The advantage of the method used is evident upon examination of (8)–(11). If the wires were precisely at 45° to the vector **Q**, all the a_{ij} will equal the b_{ij}, and all the correction terms to the right of the measured output terms (in square brackets) go to zero. In fact, these corrections were small, but had to be retained as the effective wire angles varied by the amount $\pm 6°$ depending on wire, probe position and local pitch angle. Thus, the full equations (8)–(11) were retained in the final data reduction procedure, which also contained (3), to convert the output into final form in terms of $\overline{c_1^2}$, $\overline{c_2^2}$, etc.

The terms containing $\overline{q_1^2}$ in (8)–(11) are potentially the largest correction factors as $\overline{q_1^2} \sim 10^{-2} \times U_{\text{ref}}^2$ compared to the value of $\overline{q_2^2}$ and $\overline{q_3^2}$, which are two to four times smaller than $\overline{q_1^2}$ and $\overline{q_1 q_2}$ and $\overline{q_3 q_2}$, which are of the order $10^{-3} \times U_{\text{ref}}^2$ and $10^{-4} \times U_{\text{ref}}^2$, respectively. However, the single wire measurements of $\overline{q_1^2}$, when used to evaluate these correction terms in the final data reduction, were of sufficient accuracy because of the small magnitudes of the correction term coefficients.

In (9)–(11) for the cross-stress correlation $\overline{q_3 q_2}$, the correlation $\overline{q_3 q_1}$ appears in the last correction term. Because the pitch angle β is small, $\overline{q_3 q_1}$ is nearly equal to $\overline{c_3 c_1}$, the correlation of the velocity fluctuations along and normal to **C** (see (3*f*)). No attempt was made to measure this term during the original experiments. $\overline{q_3 q_1}$ was set equal to zero. Hence $\overline{c_3 c_1}$ was also close to zero.

It is possible to take other positions with regard to the correlation of fluctuations in the plane of the wall. If the turbulence field is assumed to take up the symmetry conditions required of 'infinite' swept flow, then the correlation of the perpendicular fluctuation components u, normal to, and w, parallel to the step should go to zero, i.e. $\overline{uw} = 0$ close to the step. On the other hand, upstream, where the flow is two-dimensional, the correlation of components $\tilde{u}$ and $\tilde{w}$, parallel and normal to the reference line, should be zero, i.e. $\overline{\tilde{u}\tilde{w}} = 0$. Data reduction using all three assumptions (i.e. $\overline{q_3 q_1} = 0$, $\overline{\tilde{u}\tilde{w}} = 0$, $\overline{uw} = 0$) indicated that no significant changes in results were detected when the assumption $\overline{\tilde{u}\tilde{w}} = 0$ was substituted for $\overline{q_3 q_1} = 0$, but at the downstream stations wildly different values in $\overline{q_3 q_2}$ occurred in the outer parts of the layer when $\overline{uw} = 0$ was assumed. Near the wall ($y < 0{\cdot}5$ in.) all assumptions gave nearly equal values of $\overline{q_3 q_2}$. Upstream, at station 12, the assump-

tion $\overline{uw} = 0$ gave, as expected, results that were obviously in error. Subsequent direct measurements† of $\overline{c_3c_1}$ vindicated the original assumption that $\overline{q_3q_1} = 0$. The measured values of $(\overline{c_3c_1}/U_{\text{ref}}^2)$ were less than 3×10^{-4} in magnitude, too small to contribute a significant correction to $\overline{q_3q_2}$ calculated from (11).

Complete profile measurements were taken at downstream stations 2 and 4 and at 7, the upstream station.‡ The results are plotted in figures 15–18.

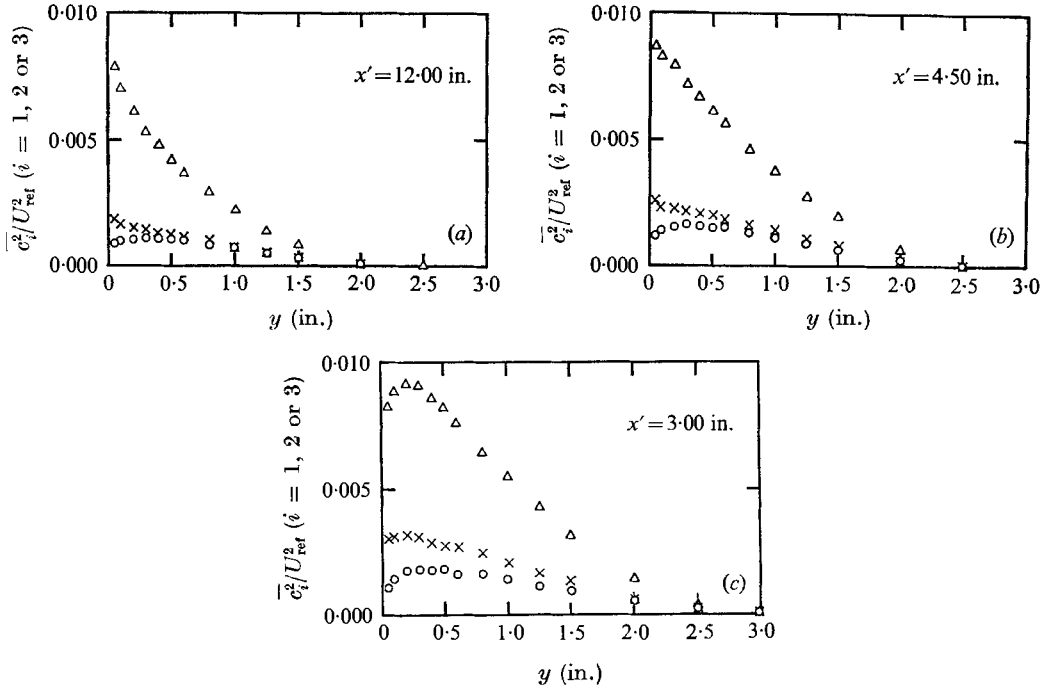

FIGURE 15. Components of turbulence intensity: △, $\overline{c_1^2}/U_{\text{ref}}^2$; ○, $\overline{c_2^2}/U_{\text{ref}}^2$; ×, $\overline{c_3^2}/U_{\text{ref}}^2$. (*a*) At $x' = 12{\cdot}00$ in. (*b*) At $x' = 4{\cdot}50$ in. (*c*) At $x' = 3{\cdot}00$ in.

The results of greatest interest are the angles θ_τ, of the shear-stress vector shown for the downstream stations in figures 18 (*a*) and (*b*). Upstream at $x' = 12$ in. the values of θ_τ should have equalled zero, but over almost the whole layer ($0{\cdot}1 < y < 1{\cdot}50$ in.) the measured values of $\theta_\tau \approx +2°$, and at the closest point to the wall, $y = 0{\cdot}50$ in, $\theta_\tau = +5{\cdot}5°$. On the basis of these results, it was concluded that fixed errors of from 0·3 to $1 \times 10^{-4}\ U_{\text{ref}}^2$ could occur in the $\overline{c_3c_2}$ results. The source of these errors is unknown, but at the downstream stations, bars have been drawn below the θ_τ data points in figures 18 (*a*) and (*b*) to indicate the downward shift required to account for the θ_τ errors noted at the upstream station.

The experimental uncertainties in the other measured turbulence quantities are estimated to be less than ± 10% of their peak values except possibly for the points closest to the wall ($y \leqslant 0{\cdot}1$ in.), where uncertainties may be as high as ± 15%.

† Conducted on the original apparatus by Mr Gordon Hutchings.

‡ Valuable check measurements for $y = 0{\cdot}5$ and 1·0 in. at stations 2, 4, 5, 6 and 7 were carried out independently by Mr Ian Hogg.

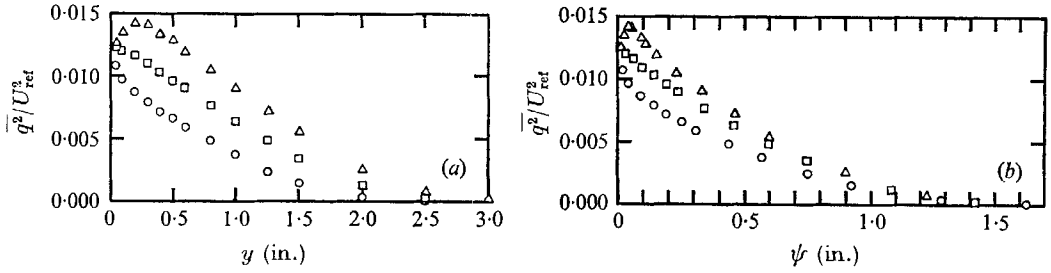

FIGURE 16 (*a*), (*b*). Turbulence intensity: ○, $x' = 12{\cdot}00$ in.; □, 4·50 in.; △, 3·00 in.

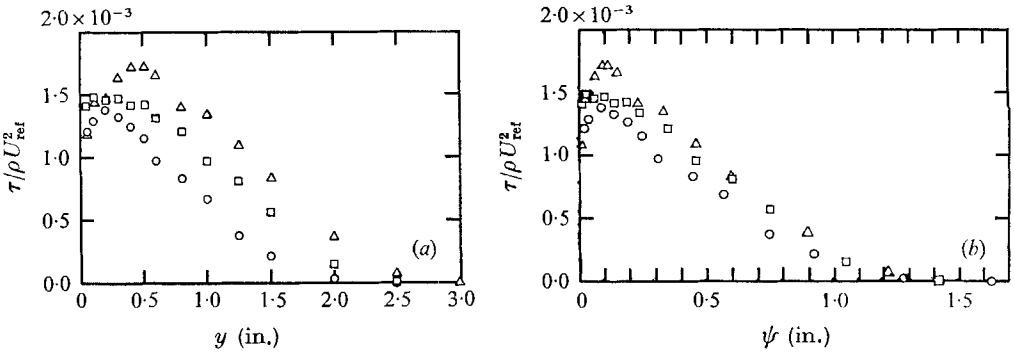

FIGURE 17 (*a*), (*b*). Turbulent shear-stress magnitude: ○, $x' = 12{\cdot}00$ in.; □, 4·50 in.; △, 3·00 in.

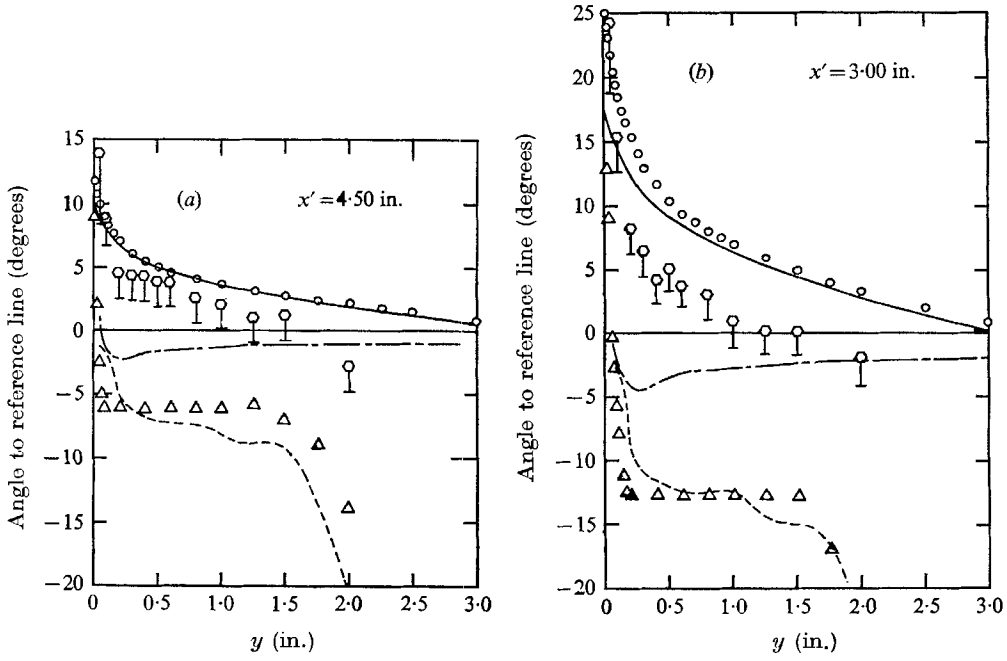

FIGURE 18 (*a*), (*b*). ○, angles of velocity θ; ⬡, shear-stress θ_τ; △, mean velocity gradient vectors relative to the tunnel reference line. Computation from §5 shown as lines: —, yaw angle θ; –·–·–, shear-stress angle θ_τ; – – – –, mean velocity gradient vector angle. (*a*) At $x' = 4{\cdot}5$ in. (*b*) At $x' = 3{\cdot}0$ in.

The results of the measurements may again be more easily interpreted when plotted *vs.* stream function as indicated in figures 16 and 17. The turbulence intensity $\overline{q^2}$ and shear-stress τ appear to grow too rapidly into the outer layers when plotted against distance from the wall. However, when examined for changes along mean streamlines in figures 16(*b*) and 17(*b*), it is seen that they have increased only slightly in the streamwise direction, except near the wall. Both $\overline{q^2}$ and τ exhibit a peculiar peak just below $y = 0{\cdot}5$ at $x' = 3{\cdot}0$ in. At first this peak was believed to be the result of some experimental error, but later calculations (§5) indicated that the peak could result from reduction of turbulent dissipation due to the concave upward curvature of the mean flow in the wall normal plane.

5. Calculations

An attempt to predict the mean velocity and shear-stress profiles was carried out using Bradshaw's (1969) three-dimensional method. The calculations were programmed in rectangular Cartesian co-ordinates where x, U and $\tau_x = -\rho\overline{uv}$ were set normal to the step and z, W and $\tau_z = -\rho\overline{wv}$ parallel to the step, see figure 3. The conditions of 'infinite' swept flow were assumed so that all derivatives with respect to the z direction were set to zero.

The basic equations used were the boundary-layer momentum equations,

$$\frac{DU}{Dt} = \frac{1}{\rho}\frac{\partial \tau_x}{\partial y} - \frac{1}{\rho}\frac{\partial p}{\partial x}, \tag{12}$$

$$\frac{DW}{Dt} = \frac{1}{\rho}\frac{\partial \tau_z}{\partial y}, \tag{13}$$

where

$$\frac{D}{Dt} = U\frac{\partial}{\partial x} + V\frac{\partial}{\partial y}, \tag{14}$$

and the incompressible continuity equation

$$\frac{\partial U}{\partial x} + \frac{\partial V}{\partial y} = 0. \tag{15}$$

The equation for the rate of change of the *scalar magnitude*, $\tau = (\tau_x^2 + \tau_z^2)^{\frac{1}{2}}$, of the shear-stress is

$$\frac{1}{2a_1}\frac{D\tau}{Dt} = \left[\tau_x\frac{\partial U}{\partial y} + \tau_z\frac{\partial W}{\partial y}\right] - \left[\frac{(\tau/\rho)^{\frac{3}{2}}}{L}\right] - \frac{\partial}{\partial y}\left[G\tau\left(\frac{\tau_{\max}}{\rho}\right)^{\frac{1}{2}}\right], \tag{16}$$

where $a_1 \equiv \tau/\overline{q^2}$, L the dissipation length, and G the diffusion function are defined precisely as in two-dimensional flow by Bradshaw *et al.* (1967). The equation for the rate of change of *direction* (component ratio) of the shear-stress is

$$\frac{1}{2a_1}\frac{D(\tau_z/\tau_x)}{Dt} = \frac{\tau}{\tau_x^2}\left[\tau_x\frac{\partial W}{\partial y} - \tau_z\frac{\partial U}{\partial y}\right] - G\left(\frac{\tau_{\max}}{\rho}\right)^{\frac{1}{2}}\frac{\partial}{\partial y}\left(\frac{\tau_z}{\tau_x}\right). \tag{17}$$

It is seen that a dissipation term does not appear in (17). Hence, near the surface where rates of change of shear-stress and diffusion terms become small, i.e. where a scalar 'eddy viscosity' model might be appropriate, (1) should be valid.

A program† for solving these equations was constructed to compute results starting with the initial conditions provided by the U, W, τ_x and τ_z data at station 7, $x' = 12{\cdot}00$ in. The numerical technique and methods for satisfaction of boundary conditions were very similar to those of Nash (1969).

Bradshaw (1969) carried out calculations for this case using the wall values of the static pressure gradients $(\partial p/\partial x)_w$. His results deviated appreciably from the measured results in the outer flow for $y > 1{\cdot}00$ in. from the wall because of the large pressure gradients normal to the wall. To overcome this problem, the local value of $\partial p/\partial x$, determined as a function of x and y from the data in figure 4, was fed into the computer program.

The computed results for limiting wall streamline angle and wall shear-stress are shown in conjunction with the data in figures 6 and 11, respectively. Calculated angles of velocity vector θ, shear-stress θ_τ, and mean velocity gradient for the stations at $x' = 4{\cdot}5$ and $3{\cdot}0$ in. are given in figure 18 (*a*), (*b*). The computed yaw angles θ, like the values of the velocity magnitude Q (not shown), were in good agreement with the measurements even though the shear-stress angle θ_τ is not accurately predicted in the inner half of the layer. Clearly, the reason for this apparent inconsistency must be the weak influence of the small cross-flow shear-stresses ($\tau \sin\theta_\tau < 1{\cdot}5 \times 10^{-4} \rho U_{\text{ref}}^2$) on the establishment of the mean velocity field in such a strong pressure gradient situation.

Within the restrictions and assumptions implied by use of (16), Bradshaw (1969*a*) developed a first-order correction for the dissipation length scale L to account for the effects of wall curvature on the turbulent shear-stress. He has suggested‡ an extension to this method for three-dimensional layers, which for concave surfaces consists of multiplying the flat plate L value by a factor $(1 - 4{\cdot}5Ri)$. Ri is the first-order approximation for the Richardson number, i.e.

$$Ri = \frac{2U}{R} \frac{(\tau_x/\rho)^{\frac{1}{2}}}{(\tau/\rho)} L,$$

where R (negative for concave surfaces) is the surface radius of curvature of a developable surface. U and τ_x are taken normal to the surface generators. In the experiment the surface was flat, but, due to flow up over the step, the mean streamlines had concave curvature over most of the outer layers, see figure 13. Values of R/δ, estimated from the data, ranged from approximately -250 at $x' = 12{\cdot}00$ in. to -5 at $x' = 3{\cdot}00$ in. A recalculation of the results using the curvature correction factor to modify L produced significant change in only one calculated quantity, the shear-stress magnitude τ. The uncorrected calculations did not show the peak value of $\tau/\rho U_{\text{ref}}^2 = 1{\cdot}74 \times 10^{-3}$ at $y = 0{\cdot}5$ in. and $x' = 3{\cdot}00$ in. (see figure 17 (*a*)), whereas the curvature corrected results show this peak in the right location and with nearly the exact experimental magnitude. The peaking of the $\overline{q^2}$, figure 16, and the τ profile at the $x' = 3{\cdot}0$ in. station had not

† Coded and run by Mr A. J. Wheeler of Stanford.

‡ Private communication and Bradshaw (1969). The general form of the factor is $(1 + \beta Ri)^{-1}$ or $(1 - \beta Ri)$, where $\beta = 7$ for convex ($R > 0$) surfaces or 4·5 for concave ($R < 0$) surfaces. It probably should not be used for $|Ri| > 0{\cdot}2$. In our calculation $|Ri|$ became large in the outer part of the layer and the form $(1 - 4{\cdot}5\,Ri)$ had to be chosen to avoid the calculation of negative values of L.

previously been understood, but these peaks are now believed to be caused by the curvature induced reduction of turbulent dissipation (i.e. increase in dissipation length scale L).

The fact that these first-order curvature corrections do not essentially modify the other calculated results is not surprising. L does not enter directly into the shear-stress direction calculation (17), and the mean velocity field development depends primarily upon the strong pressure gradients of this flow; it is only secondarily dependent upon changes of shear-stress along the mean streamlines.

6. Conclusions

Even when the most pessimistic estimates concerning error in the measured shear-stress angles θ_τ are considered, it is believed that the present measurements demonstrate the possibility of substantial deviation of the turbulent shear-stress direction from the mean velocity gradient direction. For example, angular differences of the order 15°–20° between these two directions are shown to exist at $x' = 3{\cdot}0$ in. in figure 18(*b*). Furthermore, the assumptions of Bradshaw for computing the shear-stress direction gave results that, although closer to the measurements, are opposite in trend over most of the layer. That is, in the outer $\frac{8}{10}$ of the layer the calculated results for θ_τ are increasingly negative as the wall is approached, while the measurements increase in the positive sense. It has already been shown that a first-order correction for the effects of mean streamline curvature in the plane normal to the wall cannot account for this difficulty.

It is not surprising to find that the isotropic eddy-viscosity concept, which predicts the equivalence of shear-stress angle and mean velocity gradient angle, should fail for the severe conditions of this experiment. However, it is much more difficult to understand the failure of the rate equation approach of Bradshaw to at least predict the correct trends for the variaton of θ_τ with y. Possibly, our current ideas about the nature of three-dimensional turbulence are in part wrong. On the other hand, the key to understanding the contradictory results of theory and experiment may lie in some as yet unknown difficulty with the experimental conditions. Further general speculation, unsupported by improved theory or new data, cannot at this time resolve the issue.

Finally, although this study raises some new questions about the models currently in use for representation of three-dimensional turbulent shear stress, the current differential computing methods show great promise for engineering computations of the mean flow field. The success of these methods in mean field prediction for this case should not, however, be taken as absolute proof of their generality, since the flow was so dependent upon the pressure field that quite large errors in computed shear-stress direction had a negligible effect on the computed mean flow.

The experimental part of this study was carried out in the Aerodynamics Division of the National Physical Laboratory, Teddington, England. The financial assistance, in the form of a Visiting Research Fellowship from the laboratory, and the material assistance of the staff, is gratefully acknowledged.

In particular, I express my special thanks to Dr Pankhurst, the Division Superintendent, and to Peter Bradshaw, with whom I worked. Finally, I thank the Honours Committee of the American Society of Mechanical Engineers for a Freeman Fellowship, which financed my travel to and from England.

REFERENCES

BRADSHAW, P. 1965 *N.P.L. Aero Rep.* 1171.

BRADSHAW, P. 1969 *N.P.L. Aero Rep.* 1286.

BRADSHAW, P. 1969*a* *J. Fluid Mech.* **36**, 177.

BRADSHAW, P., FERRIS, D. H. & ATWELL, N. P. 1967 *J. Fluid Mech.* **28**, 593.

BRADSHAW, P. & GALEA, P. V. 1967 *J. Fluid Mech.* **27**, 111.

BRADSHAW, P. & JOHNSON, R. F. 1963 *N.P.L. Notes on Applied Science*, **33**.

BRADSHAW, P. & TERRELL, M. G. 1969 *N.P.L. Aero Rep.* 1305.

BRYER, D. W., WALSHE, D. E. & GARNER, H. C. 1955 *Aero. Res. Counc. R. & M.* 3037.

CUMPSTY, N. A. & HEAD, M. R. 1967 *Aero. Quart.* **18**, 55, 150.

JOUBERT, P. N., PERRY, A. E. & BROWN, K. C. 1967 In *Fluid Mechanics of Internal Flow* (ed. G. Sovran). Amsterdam: Elsevier.

KLINKSIEK, W. F. & PIERCE F. J. 1969 *American Soc. Mech. Eng., Paper* 69–FE–24.

MASKELL, E. C. 1955 *Royal Aircraft Establishment, Farnborough, Rep.* 2565.

NASH, J. F. 1969 *J. Fluid Mech.* **37**, 625.

PERRY, A. E. & JOUBERT, P. N. 1965 *J. Fluid Mech.* **22**, 285.

PIERCE, F. J. & KROMMENHOEK, D. J. 1968 *Army Research Office, Durham, Project* 6858E, *Interim Tech. Rep.* 2. (Available from DDC as AD 680 973.)

TOWNSEND, A. A. 1956 *The Structure of Turbulent Shear Flow.* Cambridge University Press.